Simultaneous creation of metal nanoparticles in metal organic frameworks via spray drying technique

Accepted Manuscript

Simultaneous Creation of Metal Nanoparticles in Metal Organic Frameworks via Spray Drying Technique

Nadia Gholampour, Somboon Chaemchuen, Zhi-Yi Hu, Bibimaryam Mousavi, Gustaaf Van Tendeloo, Francis Verpoort

PII: S1385-8947(17)30629-0
DOI: http://dx.doi.org/10.1016/j.cej.2017.04.085
Reference: CEJ 16839

To appear in: *Chemical Engineering Journal*

Received Date: 27 February 2017
Revised Date: 11 April 2017
Accepted Date: 17 April 2017

Please cite this article as: N. Gholampour, S. Chaemchuen, Z-Y. Hu, B. Mousavi, G. Van Tendeloo, F. Verpoort, Simultaneous Creation of Metal Nanoparticles in Metal Organic Frameworks via Spray Drying Technique, *Chemical Engineering Journal* (2017), doi: http://dx.doi.org/10.1016/j.cej.2017.04.085

Simultaneous Creation of Metal Nanoparticles in Metal Organic Frameworks via Spray Drying Technique

Nadia Gholampour[a], Somboon Chaemchuen[a], Zhi-Yi Hu[d], Bibimaryam Mousavi[a], Gustaaf Van Tendeloo[a,d], Francis Verpoort[a,b,c,*]

[a] State Key Laboratory of Advanced Technology for Materials Synthesis and Processing, Wuhan University of Technology, Wuhan, China

[b] *National Research Tomsk Polytechnic University, Lenin Avenue 30, 634050 Tomsk, Russian Federation*

[c] Ghent University Global Campus, Songdo 119 Songdomunhwa-Ro, Yeonsu-Gu, Incheon 406-840, South Korea.

[d] EMAT (Electron Microscopy for Materials Science), University of Antwerp, Groenenborgerlaan 171, 2020 Antwerp, Belgium

E-mail: Francis.verpoort@ugent.be / Francis@whut.edu.cn

ABSTRACT

In-situ fabrication of palladium(0) nanoparticles inside zeolitic imidazolate frameworks (ZIF-8) has been established via one-step facile spray-dry technique. Crystal structures and morphologies of the Pd@ZIF-8 samples are investigated by powder XRD, TEM, SAED, STEM, and EDX techniques. High angle annular dark field scanning transmission electron microscopy (HAAD-STEM) and 3D tomographic analysis confirm the presence of palladium nanoparticles inside the ZIF-8 structure. The porosity, surface area and N_2 physisorption properties are evaluated for Pd@ZIF-8 with various palladium contents. Furthermore, Pd@ZIF-8 samples are effectively applied as heterogeneous catalysts in alkenes hydrogenation. This straightforward method is able to speed up the synthesis of encapsulation of metal nanoparticles in metal organic frameworks.

Keywords: Spray-drying, Metal organic frameworks, Metal nano-particles, Alkene hydrogenation

1. Introduction

Metal organic frameworks (MOFs) are a class of porous materials formed by assembling inorganic ions as metal clusters bridging with organic compounds as ligand building a metal organic material;[1, 2] which opens up potential for plenty of applications including drug delivery,[3, 4] contrast agents,[5] sensor technology,[6] functional membranes and thin film[7, 8], as well as traditional storage,[9] separation,[10, 11] and catalysis applications.[12, 13] The catalytic applications of

MOFs have received so much attention due to their adaptable properties *e.g.* high porosity, the versatile tailor design structure, easy separation from reaction mixture, chemical and thermal stability.[12, 13]

Recently, it has been shown that inner surface of channels and cavities of MOF materials can be a supporting host matrix for nanoparticles, thereby affecting their catalytic activities and selectivity in reactions. There are two strategies to fabricate nanoparticles inside MOFs; a) post-synthesis incorporation of nanoparticles into as-prepared MOFs which includes numerous preparative approaches such as liquid and incipient wetness impregnation,[14, 15] solid grinding,[16] gas phase methods[17] and microwave irradiation,[18] and b) *in-situ* encapsulation of pre-synthesized nanoparticles in MOFs. It is worth to mention that nonselective deposition of nanoparticles at the outer surface of MOFs crystals in all post-synthesis procedures is unavoidable.[19, 20] To circumvent this limitation, recently, a double solvent impregnation method (DSM) followed by using H_2 or high-concentration of $NaBH_4$ to reduce the metal precursors, was applied to fabricate metal nanoparticles throughout the interior pores of MOFs.[21, 22] In this regard, Sanchez *et al.*[23] demonstrated that the spray drying method is a versatile, low-cost and rapid procedure enabling not only simultaneous synthesis and assembly of different types of nano-MOFs, with diameters smaller than 5μm without employing secondary immiscible solvent or surfactant, but also proved that the spray-drying procedure enables greater compositional complexity of hollow MOF superstructures. Moreover, Maspoch *et al.* [24] synthesized various kinds of MOFs including UiO-66, Fe–BTC/MIL-100 and $[Ni_8(OH)_4(H_2O)_2(L)_6]_n$ by applying a spray-drying flow-assisted process in which MOFs assembled from high-nuclear secondary building units (SBUs) as compact microspherical superstructures (beads). Additionally, the spray drying technique was employed for post modification of amine-terminated UiO-66-NH_2 and aldehyde-terminated ZIF-90 to achieve the Schiff-base condensation between an amine and an aldehyde in the MOF structure.[25]

ZIF-8 is one of the most widely studied MOF families which is constructed by bridging of Zn clusters with 2-methylimidazole as ligand. These ZIFs possess a permanent porosity, high thermal stability and remarkable chemical resistance to boiling alkaline water and organic solvents a good candidate to host nanoparticles.[26] In recent years, various strategies were applied to encapsulate palladium nanoparticles inside the ZIF-8 structure in which these composites are synthesized during multi-steps and/or by using stabilizer for palladium particles.[27, 28]

Catalytic hydrogenation is of a great interest in a variety of industrially important processes such as alkene hydrogenation to convert naphtha via fluid catalytic cracking (FCC) into gasoline [29, 30] or selective hydrogenation of polyunsaturated fatty acid-

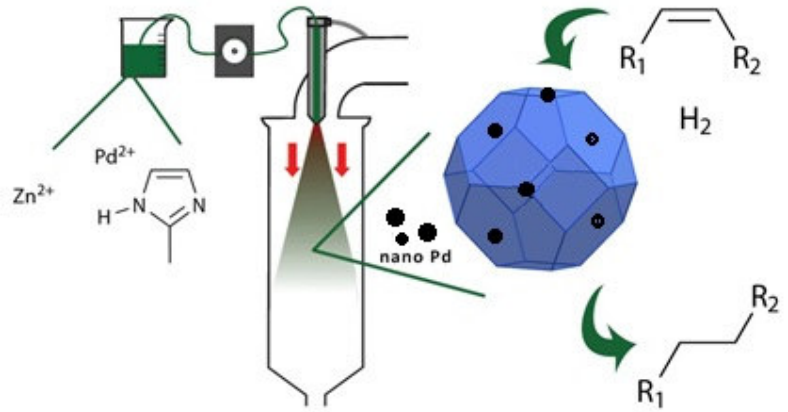

Fig. 1. Schematic illustration of the *in-situ* synthesis of Pd nanopaticles inside ZIF-8. Pd@ZIF-8 is applied as heterogeneous catalyst in alkene hydrogenation.

methyl esters (FAMEs) to the corresponding mono-unsaturated derivatives. Palladium supported on various carriers is a well-known heterogeneous catalyst applied in hydrogenation reactions.[31-33]

In this study, we present the first case of simultaneous fabrication of palladium(0) particles inside the ZIF-8 (Pd@ZIF-8) via spray dry technique without applying any kind of surfactant or stabilizer leading to an active catalyst for alkene hydrogenation (Fig. 1). The synthesis of Pd@ZIF-8 serves as an example that displays this methodology can be applied to prepare any kind of nano-sized metal particles in ZIFs (M@ZIF) or even in MOFs (M@MOF) as long as the MOF can be spray dried.

2. Experimental

2.1. Chemicals

2-methylimidazole was purchased from Sigma-Aldrich Chemical Co., Ltd. Zinc acetate, palladium acetate, styrene, cyclooctene and phenylacetylene were purchased from Aladdin Chemical Co., Ltd. Methanol was purchased from Sinopharm Chemical Reagents Co., Ltd. All chemicals and solvents were used as they are received without further purification.

2.2. Synthesis of ZIF-8 and Pd@ZIF-8

Spray drying technique was applied to synthesize ZIF-8 and Pd@ZIF-8 samples. In a typical synthesis, a solution of zinc acetate (1.765 g, 8 mmol) and palladium acetate (x mmol based on the Zn source) in distilled water (25 ml) was added to a solution of 2-methylimodazole (2-MIM) (8 mmol, 0.66 g) in distilled water (25 ml)

under stirring. The obtained solution was stirred for 1 min before feeding to the spray drying instrument. Thereafter, the obtained white suspension was continuously stirred and fed into the spray-drier (AF-88 labs Spray dryer, AFIND Scientific instrument CO., LTD.) using a spray nozzle having a diameter of 8 mm, at a feed rate of 300 ml/h, a flow rate of 160 m^3/h and an inlet temperature of 180^0C. The produced white powder was collected, washed with methanol followed by centrifugation and re-dispersion in methanol for three times. Lastly, the wet product was dried at room temperature under vacuum for 12h. The final products were collected and kept in a desiccator for further characterization. The Pd@ZIF-8 samples were synthesized similar as ZIF-8 except for the addition of Palladium acetate (x mmol based on Zinc salt).

2.3. Synthesis of ZIF-8 in the presence of melamine

A mixture of zinc acetate (8 mmol, 1.765 g), 2-methylimodazole (2-MIM) (8 mmol, 0.66 g) and melamine (0.01 mmol) in distilled water (50 ml) was stirred and spray dried (similar conditions as for spray drying of ZIF-8 and Pd@ZIF-8 samples). The produced white powder was collected, washed with methanol followed by centrifugation and re-dispersion in methanol for three times. Lastly, the wet product was dried at room temperature under vacuum for 12h. The final products were collected and kept in a desiccator for further characterization.

2.4. Catalytic hydrogenation

General procedure for catalytic hydrogenation**,** 10 mg catalyst (Pd@ZIF-8) was transferred to a 15 ml Schlenk tube under a constant H_2 flow. Thereafter, 6 ml methanol (solvent), 50 µl dodecane (internal standard) and the desired amount of styrene (substrate) (styrene/Pd = 1000, 500) were transferred into the Schlenk tube. Finally, a balloon with H_2 was attached to the Schlenk tube to maintain the H_2 atmosphere and temperature was kept at 40°C. Conversion was determined by GC following this formula: Conversion % $=\frac{[styrene]0-[styrene]t}{[styrene]0} * 100$, where $[styrene]0$ is the concentration of styrene at t=0 and $[styrene]t$ is the concentration of styrene at a given time.

2.5. Characterization

Transmission electron microscopy (TEM), high resolution transmission electron microscopy (HR-TEM), high angle annular dark field scanning transmission electron microscopy (HAAD-STEM) and energy dispersive X-ray spectroscopy (EDX) were performed on a FEI Osiris fitted with a Super-X windowless EDX detector system, operated at 200kV. Powder X- ray diffraction (PXRD) patterns of samples were

collected (Using Bruker D8 Advance diffractometer, Bragg-Brentano geometry, Cu Kα radiation) in the 2θ range 3-40°. The surface area and adsorption isotherm measurements were performed on Micromeritics instrument (ASAP2020) at 77 K using liquid nitrogen as coolant. Prior to the adsorption measurements, the samples were evacuated at 200°C under dynamic vacuum for about 3 h. The micropore surfaces were calculated by the Brunauer-Emmett-Teller (BET) and Langmuir method ($0.005 < P/P_0 < 0.05$). Fourier transform infrared (FT-IR) spectra were collected on a Perkin-Elmer Spectrum One spectrometer. The binding energies of the elements in the samples were analyzed using X-ray photoelectron spectroscopy (XPS) on a Thermo Fisher ESCALAB 250Xi. Elemental analysis was performed using ICP-AES an Optima4300DV. Substrate conversions during hydrogenation reaction were determined by GC (Agilent) with a HP-5 column and a flame ionization detector.

3. Results and Discussion

3.1. Synthesis and characterization of Pd@ZIF-8 with various loadings of palladium

The integration of palladium(0) particles into ZIF-8 was achieved in one step using spray drying technique.

Fig. 2 displays the PXRD patterns of guest free ZIF-8 sample and Pd@ZIF-8 samples with various Pd contents synthesized by spray drying method. %Pd loadings of 0.01, 0.05 and 0.1 were obtained as determined by ICP analysis. The PXRD patterns for the ZIF-8 sample and incorporated Pd@ZIF-8 samples up to 0.05%Pd loading are similar, confirming that the crystalline structure of ZIF-8 is maintained after Pd loading up to 0.05%.

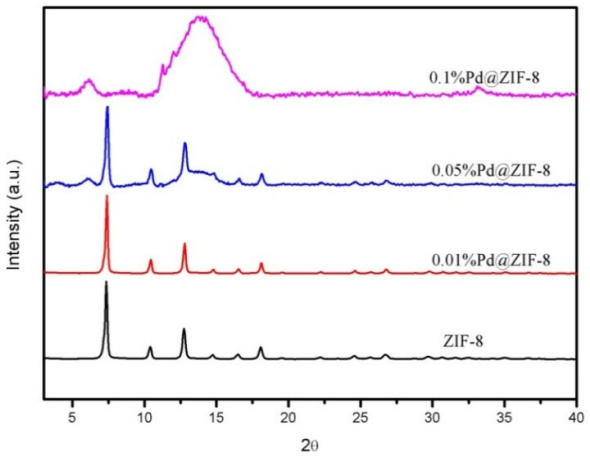

Fig. 2. The XRD patterns of ZIF-8 and incorporated Pd@ZIF-8 samples with various Pd contents.

Furthermore, the bulk Pd diffraction peaks (2θ=39°)[34] could not be found in the XRD pattern demonstrating a well dispersion and/or small crystal size of Pd particles at ZIF-8 structure. Nevertheless, with increasing the Pd content higher than 0.05% the intensity of main peak decreased and a broad peak appeared which can be assigned to the formation of amorphous structures and evading of the crystalline structure. This phenomenon can be observed from Fig. 2, the XRD pattern of 0.1%Pd@ZIF-8 shows a broad peak (from 10°-20°) which is completely different from the XRD pattern of ZIF-8. This observation can imply that introducing too much Pd in the synthesis of ZIF-8 resulted in the formation of an amorphous phase in the product which coincides with BET and N_2-physisorption analysis.

The surface area and porosity properties for ZIF-8 and Pd@ZIF-8 samples with different Pd content were measured by N_2 adsorption at 77K (see Fig. 3). A type I isotherm with an appreciable increase in N_2 uptake at a relative low pressure was observed for ZIF-8 and Pd@ZIF-8 sample with 0.01%Pd content confirming the formation of a microporous structure. However, by increasing the palladium content a sharp decrease in the N_2 uptake is observed. The surface area of the samples measured by Brunauer–Emmett–Teller (BET) method and Langmuir, and porosity properties (pore volume and pore size) of the samples measured by Horvath-Kawazoe (H-K) method are summarized in Table 1.

Surprisingly, a higher N_2 uptake and as a result a superior surface area and porosity (larger pore volume) was found for the 0.01%Pd@ZIF-8 sample compared to ZIF-8. We reasoned that this phenomenon originates from the presence of the acetate anion, which acts as a weak base and hence is responsible for deprotonating the ligand which coordinates with the metal ion. Variation parameters including employing some additives as weak-base can accelerate the deprotonation of the ligand (imidazole) in the medium solution which can influence the crystal growth and properties of ZIF-8 as well.[35, 36] This is in agreement with the recent report investigating the pH influence on the textural properties of MOFs.

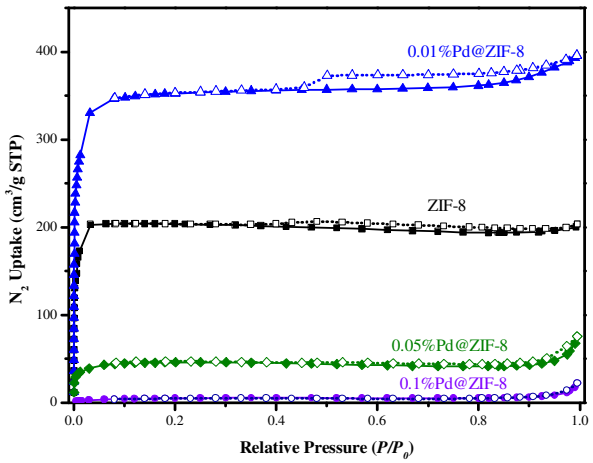

Fig. 3. N_2 adsorption-desorption isotherms of ZIF-8 and Pd@ZIF-8 with various Pd contents.

It is demonstrated that applying melamine (which is considered as a weak-base) and keeping the reaction medium within a particular pH range led to the formation of MOFs with highly crystalline structures having higher surface areas compared with MOFs synthesized without using melamine while the characterization confirms the absence of melamine in the pores of as-synthesized MOFs.[37, 38] Additionally, the weak-base additives act as accelerator for nucleation and deprotonation of the bridging Hmim ligand (deprotonation modulation) in ZIF-8 synthesis.[35] Therefore, increasing the pH value of the spray draying feed solution by using palladium acetate as acetate source, representing a weak-base in the solution, could be responsible for a higher N_2 uptake of the final 0.01%Pd@ZIF-8 sample.

Regarding the role of the pH influence in the reaction medium (feed solution), this effect was investigated by adding a small amount of melamine (0.01mmol) in the ZIF-8 feed solution. Indeed, addition of melamine to the ZIF-8 feed solution resulted in a ZIF-8 sample exhibiting a higher N_2 uptake, a higher surface area and a larger pore volume in comparison to the ZIF-8 which is synthesized without applying any kind of base. (see Fig. S1). This experiment confirmed that the addition of acetate (weak-base) originating from the Pd source could increase the surface area of 0.01%Pd@ZIF-8. Accordingly, Kim *et al.*[37] revealed that controlling the pH in the synthesis of MOF is crucial. They reported that a high pH value resulted in the formation of complicated crystalline products (impure phases) such as oxo- or hydroxo-polynuclear zinc(II) clusters *etc*., which led to a smaller surface area for the MOF. Moreover, it is reported that in the case of applying a much higher amount of weak-base compound the nucleation and crystal growth is expected to be retarded

during the ZIF-8 synthesis.[39] Experiments in this work demonstrate that a low amount of base in the reaction medium assists in the formation of crystalline structures. On the contrary, increasing the Pd loading by rising the amount of Pd-acetate and hence the amount of acetate (weak base), gives rise to the formation of complicated crystalline products (impure phases) and consequently poor textural properties, such as low crystallinity (see XRD in Figure 2), low N_2 uptake, surface area and porosity of the final product (Fig. 3 and Table 1).

Table 1
Surface area and porosity properties of spray dried ZIF-8 and Pd@ZIF-8 with various Pd loadings.
* calculated by H-K method

Samples	BET (m^2/g)	Langmuir (m^2/g)	Pore size* (Å)	Pore volume* (cm^3/g)
ZIF-8	825	909	12.75	0.31
0.01%Pd@ZIF-8	1422	1568	12.65	0.54
0.05%Pd@ZIF-8	183	203	12.86	0.07
0.1%Pd@ZIF-8	17	19	20.5	0.007

Remarkably, the surface area and pore volume for Pd@ZIF-8 samples (except for the sample contains 0.01% Pd) are less compared to pure ZIF-8 which is more noticeable for the sample 0.1%Pd@ZIF-8. According to the physisorption data (Fig. 3), (no N_2 uptake at low P/P_0), 0.1%Pd@ZIF-8 sample is not microporous and BET surface area (and the pore volume) decreased significantly from 825 m^2/g (V_m: 0.31 cm^3/g) for pure ZIF-8 to 17 m^2/g (V_m: 0.007 cm^3/g) for 0.1%Pd@ZIF-8. This phenomenon most probably is due to the formation of more impurities and amorphous phase which is a result of more acetate present in the feed solution, as explained previously.

Obviously, for the synthesis Pd@ZIF-8 via spray drying process, a loading higher than 0.05% palladium in the ZIF-8 structure will result in the formation of amorphous structures as it is demonstrated by XRD, HAADF-STEM and N_2 adsorption analysis.

Transmission electron microscopy (TEM) and high angle annular dark field scanning transmission electron microscopy (HAADF-STEM) images were effectively applied to investigate the morphology of ZIF-8 bulk and the position of the Pd nano-particles in or out the ZIF-8 structure. In the HAADF-STEM image of the 0.05%Pd@ZIF-8 sample, the ZIF-8 crystal bulk can be observed and verified by SAED (Fig. S2a). The corresponding HAADF-STEM-EDX mapping shows that the Pd nanoparticles are homogeneously dispersed in the ZIF-8 crystal bulk (Fig. S2b,

e-f). The transmission electron microscopy (TEM) images at low magnification show that the size of ZIF-8 crystals ranges from 500nm to 3μm (Fig. S2a). The HR-TEM image indicates that the sizes of encapsulated Pd particles are in the range of 2-10 nm (Fig. S3). The XRD of bulk Pd (2θ=39°)[34] could not be detected in the XRD pattern demonstrating a good dispersion (no accumulation to bulk phase of Pd) and/or small crystal size of Pd particles at ZIF-8. However, for higher Pd loading a poor textural crystallinity and/or properties was observed. Moreover, it is worth noting that TEM and corresponding SAED patterns of 0.1%Pd@ZIF-8 sample (Fig. S4) demonstrates that this sample consists of both crystalline and amorphous phase. All these TEM results are highly in agreement with the XRD patterns and N_2 physisorption presented in Fig.2 and Fig.3 respectively._

Additionally, in order to investigate whether the Pd nanoparticles can be embedded in the ZIF-8 network via this spray drying technique, we first reduced the Pd content to 0.0001% and this sample is characterized by HADDF-STEM technique. As it is illustrated in Fig. 4a, the Z-contrast high angle annular dark field scanning transmission electron microscopy (HAADF-STEM) image shows a strongly faceted ZIF-8 particle. The corresponding selected area electron diffraction (SAED) pattern of the whole ZIF-8 bulk, displayed in Fig. 4a inset, indicates that the particles is one single crystal, imaged along the [121] zone axis orientation. The corresponding EDX spectrum and mapping results of the same particle, presented in Fig. 4b-e, reveal that the Pd nanoparticles are randomly and homogeneously distributed throughout the whole ZIF-8 bulk. In Fig.4f, HAADF-STEM image of a typical Pd@ZIF-8 is demonstrated. These two- dimensional (2D) (S)TEM results prove that the bulk consists of a highly crystalline ZIF-8 network with Pd nanoparticles. However, these 2D images do not reveal the 3D location of the Pd nanoparticles with respect to the ZIF-8 bulk. This can be retrieved through electron tomography, a technique in which several 2D projections are combined into a 3D reconstruction using a mathematical reconstruction algorithm.

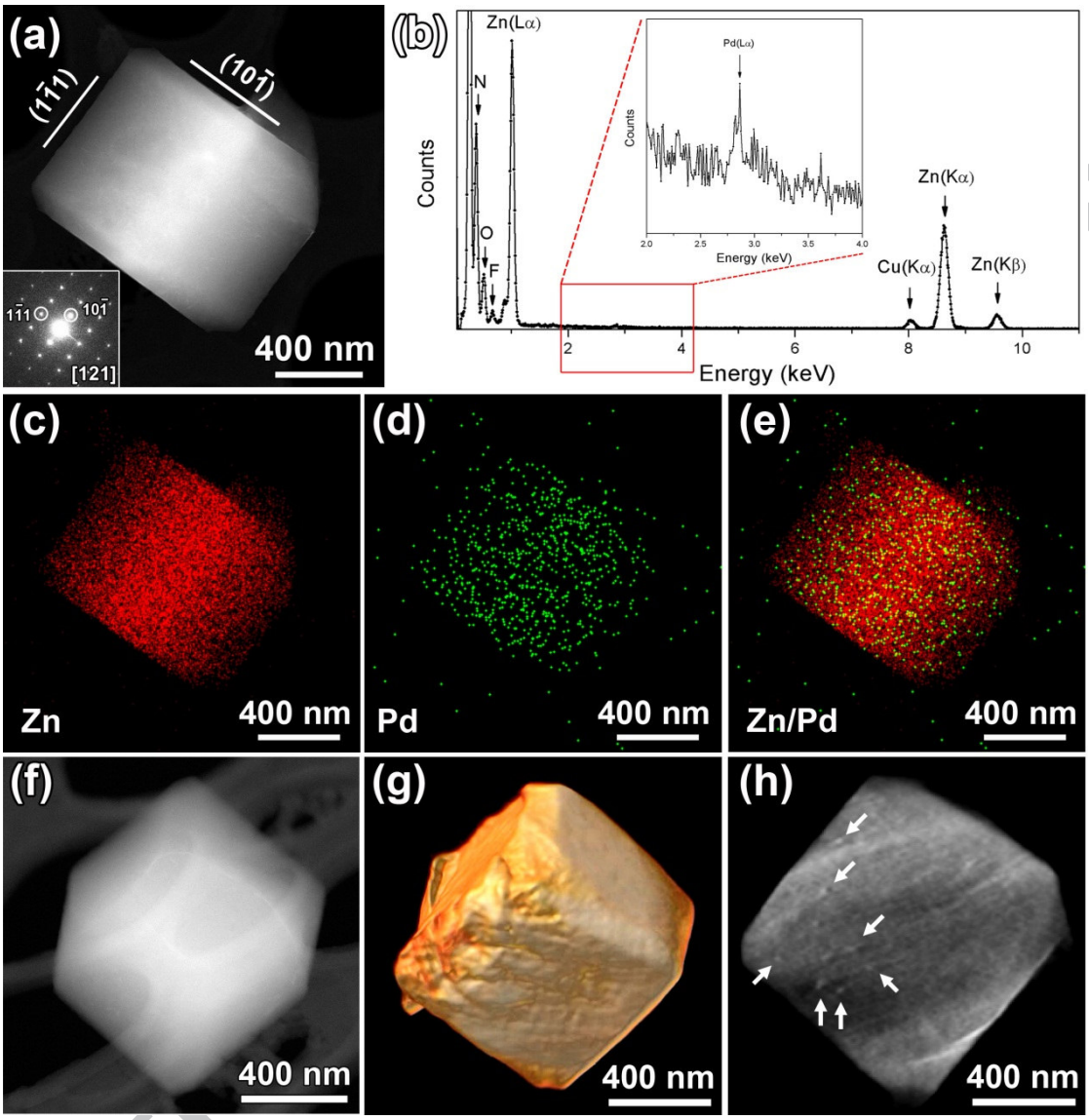

Fig. 4. (a) HAADF-STEM image of a Pd@ZIF8 bulk, and corresponding SAED pattern (inset), (b) corresponding full EDX spectrum and detailed EDX spectrum (inset), (c-e) corresponding EDX mapping results, (f) HAADF-STEM image of another typical Pd@ZIF-8 bulk, (g) 3D tomographic reconstruction of the Pd@ZIF-8 particle, (h) a slice through the Pd@ZIF-8 particle from the 3D tomographic reconstruction.

Therefore, HAADF-STEM electron tomography (Fig. 4g-h), Video-Tomo in Supporting Information) was carried out to find out the position of Pd nanoparticles. The volume reconstruction (Fig. 4g) demonstrates the 3D morphology of the ZIF-8 bulk with its typical crystal structure. To achieve a better visualization of location of the Pd nanoparticles, a slice through the bulk is shown in Fig. 4h. Because of the Z-contrast of HAADF-STEM, the Pd nanoparticles are easily distinguished through their higher intensity compared to the ZIF-8 component (indicated by white arrows in

Fig. 4h). These images clearly demonstrate that the Pd nanoparticles are *within* the ZIF-8 network.

In summary, Pd nanoparticles are homogeneously distributed inside the ZIF-8, but as the Pd content increases, more Pd nanoparticles are aggregated on the surface of the ZIF-8 bulk, and more amorphous phase is obtained via this spray drying synthetic technique.

As it is illustrated in the FT-IR spectrum corresponding to as-synthesized ZIF-8 (Fig. S5), the absorption band for Zn–N stretching mode is at 427 cm^{-1}. The C–N absorption bands can be observed in the region from 1147 to 1312 cm^{-1}. The 1591 cm^{-1} band represents the C=C stretch. The two bands at 3128 and 2931 are related to the aromatic C-H and aliphatic C-H stretch of imidazole, respectively. These peaks completely match with those reported for ZIF-8 frameworks.[40, 41] Without any doubt, the FT-IR spectrum for the 0.05%Pd@ZIF-8 sample is completely similar to the ZIF-8 spectrum (see Fig. S5).

X-ray photoelectron spectra (XPS) provide valuable information on the oxidation state of the Pd and Zn in the Pd@ZIF-8. Fig. 5a represents the general survey scan of the XPS analysis revealing the existence of Pd, Zn, C and N in the ZIF-8 coated Pd. The binding energies for Pd 3d were observed at 338.1eV and 343.5eV for Pd $3d_{5/2}$ and Pd $3d_{3/2}$ respectively (Fig. 5b) which is representative for Pd in its zero oxidation state and are in excellent agreement with previously reported values for Pd^0.[42, 43] XPS analysis confirms that Pd nano-particles, which are considered to be the active site for hydrogenation reactions are present as Pd^0 inside the ZIF-8 structure. The binding energies for Zn $2p_{3/2}$ and $2p_{1/2}$ peaks appeared at 1021.48 and 1044.55 eV, respectively (Fig. 5c) and are in excellent agreement with literature data for Zn(II). [44, 45]

Additionally, the white precipitation in feed solution which is formed during spray-drying, was characterized. Fig. S6 illustrates the XRD pattern and SEM analysis of this sample which strongly confirm that no ZIF-8 structure is formed before the spray drying process.

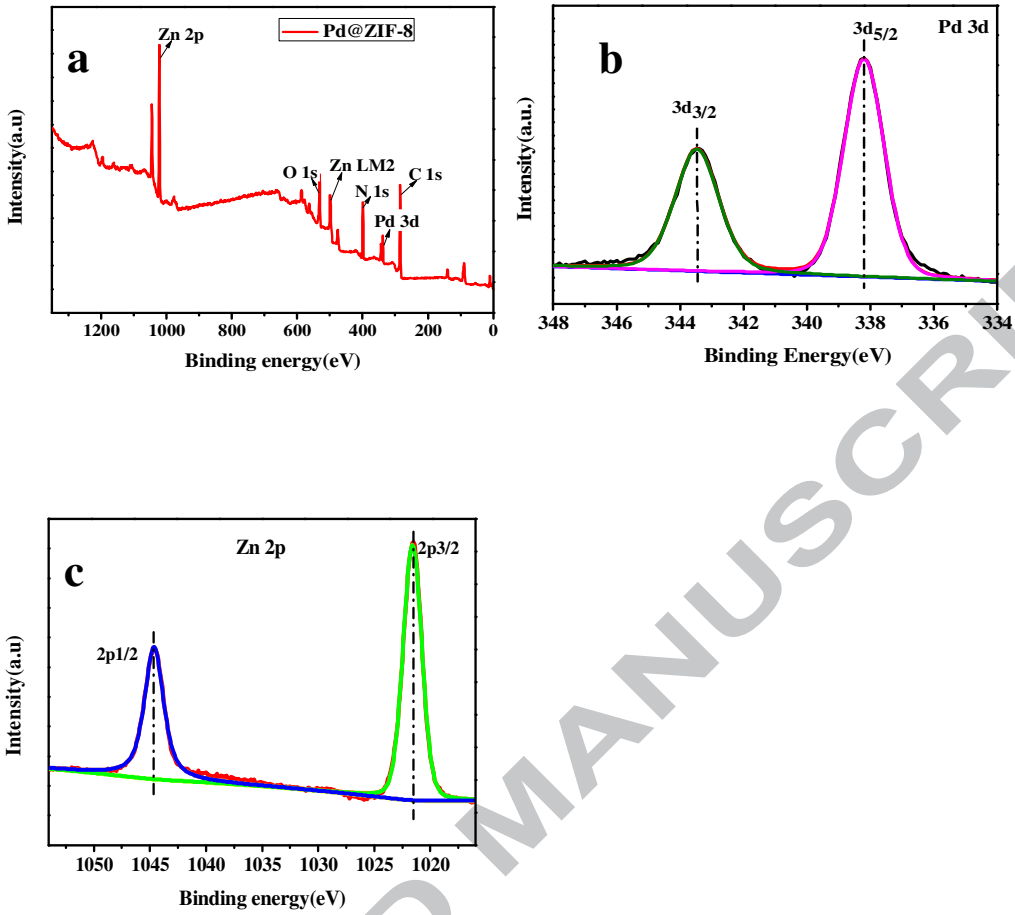

Fig. 5. (a) XPS analysis of Pd@ZIF-8 sample containing 0.05% Palladium, (b) Binding energy of Pd 3d, (c) Binding energy of Zn 2p.

3.2. Catalytic study for alkenes hydrogenation

To investigate the influence of Pd content on the catalytic performance, hydrogenation of styrene was performed using x%Pd@ZIF-8 catalysts with x = 0, 0.01, 0.05 and 0.1% of Pd (Fig. 6a). While, guest free ZIF-8 showed no activity toward hydrogenation of styrene, introduction of Pd inside the ZIF-8 exhibits an increase in catalytic performance. The best performance was achieved applying 0.05%Pd@ZIF-8. Interestingly, the catalytic activity of the composite containing 0.1% Pd was outperformed by the sample 0.05%Pd@ZIF-8 demonstrating conversion of 47% and 54% respectively. This observation can be attributed to the less crystallinity, less porosity and less surface area of the 0.1%Pd@ZIF-8 according to the XRD, N_2 adsorption and BET surface area results. Moreover, agglomeration of palladium particles at higher loading may occur, which results in lower activity.

The hydrogenation of styrene was kinetically evaluated for different Pd/Styrene ratios using the 0.05%Pd@ZIF-8 since this catalyst exhibited the best catalytic performance. The kinetic profiles for Styrene/Pd=1000 and 500 are presented in Fig.

6b. Obviously, there is a sharp increase in the initiation rate for hydrogenation of styrene as the ratio decreased from 1000 to 500 times (54% *vs*. 82% conversion).

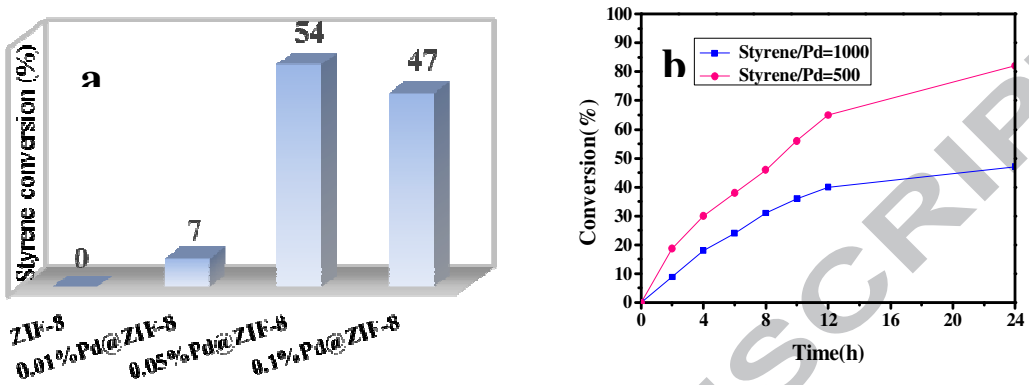

Fig. 6. (a) Catalytic hydrogenation of styrene over Pd@ZIF-8 catalysts with different Pd loading. Reaction conditions: 10 mg catalyst, Pd/Styrene=1/1000, 40°C, MeOH, 1 atm H_2, 24h. (b) The catalytic performance of 0.05%Pd@ZIF-8 for different ratio of Pd/substrate.

Table 2

Hydrogenation of alkene using 0.05%Pd@ZIF-8 as a catalyst compared with reported works.

Entry	Catalyst	Olefin	Product	TON	Ref
1	Pd@ ZIF-8	styrene[a]	ethylbenzene	410	This work
2	Pd@ ZIF-8	cyclooctene[a]	cyclooctane	75	This work
3	Pd@ ZIF-8	Phenyl acetylene[a]	Styrene	65	This work
4	Pd/ZnO@ZIF-8	cyclooctene[b]	cyclooctane	0	27
5	Pd@MOF-5	styrene[c]	ethylbenzene	99	15
6	Pd@MOF-5	cyclooctene[c]	cyclooctane	28	15

[a] Reaction condition: 10 mg catalyst, Pd/Styrene=1/500, under H_2 (atmospheric pressure, balloon), 24h, 40°C [b] 40 mg catalyst, Pd/Styrene=1/10000, under H_2 (atmospheric pressure, balloon), 24h, 35°C, [c] 50 mg catalyst, Pd/Styrene=1/100, under H_2 (atmospheric pressure), 12h and 24h for styrene and cyclooctene respectively, 35°C.

The 0.05%Pd@ZIF-8 sample was further investigated for the hydrogenation of two other olefins (cyclooctene and phenylacetylene) applying the ratio of substrate/Pd = 500 (Table 2). Remarkably, comparing with earlier reported works in which Pd nano-particles were encapsulated in MOF structures, the Pd@ZIF-8 catalyst synthesized by spray drying technique (this work) demonstrates much better turn over numbers (TON) for the same substrates. This may be attributed to a better dispersion of Pd nano-particles inside the ZIF-8 structure. Since the aggregation of metal nano particles to bulk metal cannot occur during the distribution of metal nano-particles inside the MOF. In several publications Pd^0 is considered as the catalytic site in hydrogenation reaction.[15, 46] Although in the synthesis procedure of Pd@ZIF-8 by spray drying, palladium(II) acetate is applied, XPS results revealed that Pd^0 nanoparticles are present in the ZIF-8. It is assumed that 2-methylimidazol acts as both the organic linker and the reducing agent. Since, it is reported that a redox reaction between organic linker (4,4,4-nitrilotrisbenzoate) and Pd salt resulted in the formation of Pd nanoparticles.[45] In addition, metal nanoparticles are formed in the presence of octadecylamine and it is believed that electrons can transfer from the amine to metal ions to form metal nanoparticles.[47] Therefor, similarly a redox reaction can occur between 2-methylimidazole and the palladium salt. Moreover, even acetate can act as a reducing agent which was demonstrate by Lim *et al.*[48]. In the following, more investigation has been done by pretreating the 0.05Pd@ZIF-8 sample with H_2 gas (H_2 at 150^{o}C for 2 hours) to reduce Pd salt (if there is any) to Pd NPs and then applied for hydrogenation of styrene. Interestingly, the obtained conversion for styrene was similar to the conversion obtained by the catalyst without pretreatment (85% *vs*. 82%), confirming the presence of Pd^0 inside the ZIF-8.

From industrial point of view, recyclability of heterogeneous catalysts is an important and essential feature. In order to investigate the recyclability, hydrogenation of styrene was performed on Pd@ZIF-8 sample containing 0.05% Palladium. Three consecutive hydrogenation runs were performed while after each run the spent catalyst was separated by centrifugation, washed thoroughly with methanol followed by drying in vacuum for 24h at room temperature. The conversions of three runs were 82%, 81% and 78% for the first, second and third run, respectively. According to the XRD results (Fig. S7), the crystalline structure of Pd@ZIF-8 remained unchanged after 3 runs. The surface area (BET) and pore volume of the spent catalyst are similar to the fresh sample (Table S1). Moreover, XPS analysis demonstrated that binding energies for Pd and Zn in spent and fresh sample are matching perfectly (Fig. S8).

4. Conclusions

We have presented a facile one-step synthesis of nano-sized palladium loaded at ZIF-8 structure via spry-drying. The structure of Pd@ZIF-8 remained crystalline however; the amorphous phase appeared at higher Pd content which is evident from XRD and BET analysis and HAAD-STEM images. The 0.05%Pd@ZIF-8 sample was concluded not only as the best Pd loading applied for styrene hydrogenation reaction but also as the highest loading of metal in which crystalline structure of ZIF-8 is preserved by this synthesis procedure. Vividly, HAAD-STEM analysis displayed that palladium nanoparticles are formed inside the ZIF-8 structure. Hence, spray-dry technique could be considered as an efficient, remarkable and forward method to accelerate the synthesis of Pd@ZIF-8 for industrial applications.

Acknowledgements

The authors would like to express their deep accolade to "State Key Laboratory of Advanced Technology for Materials Synthesis and Processing" for financial support. S.C. appreciates of the National Natural Science Foundation of China (303-41150231), the Fundamental Research Funds for the Central Universities (WUT: 2016IVA092) and the Research Fund for the Doctoral Program of Higher Education of China (471-40120222). N.G. thanks the Chinese Scholarship Council (CSC) for her Ph.D. study grant 2013GXZ985. Z.-Y. H and G. V.T. acknowledge the support from the EC Framework 7 program ESTEEM2 (Reference 312483).

Abbreviations

PXRD Powder X-Ray Diffraction
TEM Transmission Electron Microscopy
HR-TEM high-resolution transmission electron microscopy
SAED Selected Area Electron Diffraction
HAAD-STEM High Angle Annular Dark Field Scanning Transmission Electron Microscopy
EDX Energy Dispersive X-ray Spectroscopy
XPS X-ray Photoelectron Spectroscopy

References

[1] A. Carné, C. Carbonell, I. Imaz, D. Maspoch, Nanoscale metal–organic materials, Chemical Society Reviews 40 (2011) 291-305.
[2] M.D. Allendorf, V. Stavila, Crystal engineering, structure–function relationships, and the future of metal–organic frameworks, CrystEngComm 17 (2015) 229-246.
[3] N. Ahmad, H.A. Younus, A.H. Chughtai, F. Verpoort, Metal–organic molecular cages: applications of biochemical implications, Chemical Society Reviews 44 (2015) 9-25.

[4] P. Horcajada, R. Gref, T. Baati, P.K. Allan, G. Maurin, P. Couvreur, G. Férey, R.E. Morris, C. Serre, Metal–organic frameworks in biomedicine, Chemical reviews 112 (2011) 1232-1268.
[5] W.J. Rieter, K.M. Taylor, H. An, W. Lin, W. Lin, Nanoscale metal-organic frameworks as potential multimodal contrast enhancing agents, Journal of the American Chemical Society 128 (2006) 9024-9025.
[6] P. Kumar, A. Deep, K.-H. Kim, Metal organic frameworks for sensing applications, TrAC Trends in Analytical Chemistry 73 (2015) 39-53.
[7] A. Bétard, R.A. Fischer, Metal–Organic Framework Thin Films: From Fundamentals to Applications, Chemical reviews 112 (2011) 1055-1083.
[8] C. Scherb, A. Schödel, T. Bein, Directing the structure of metal–organic frameworks by oriented surface growth on an organic monolayer, Angewandte Chemie 120 (2008) 5861-5863.
[9] B. Li, H. Wang, B. Chen, Microporous Metal–Organic Frameworks for Gas Separation, Chemistry–An Asian Journal 9 (2014) 1474-1498.
[10] S. Chaemchuen, N.A. Kabir, K. Zhou, F. Verpoort, Metal–organic frameworks for upgrading biogas via CO 2 adsorption to biogas green energy, Chemical Society Reviews 42 (2013) 9304-9332.
[11] S. Chaemchuen, K. Zhou, N.A. Kabir, Y. Chen, X. Ke, G. Van Tendeloo, F. Verpoort, Tuning metal sites of DABCO MOF for gas purification at ambient conditions, Microporous and Mesoporous Materials 201 (2015) 277-285.
[12] A.H. Chughtai, N. Ahmad, H.A. Younus, A. Laypkov, F. Verpoort, Metal–organic frameworks: versatile heterogeneous catalysts for efficient catalytic organic transformations, Chemical Society Reviews 44 (2015) 6804-6849.
[13] J. Lee, O.K. Farha, J. Roberts, K.A. Scheidt, S.T. Nguyen, J.T. Hupp, Metal–organic framework materials as catalysts, Chemical Society Reviews 38 (2009) 1450-1459.
[14] R.J. Houk, B.W. Jacobs, F.E. Gabaly, N.N. Chang, A.A. Talin, D.D. Graham, S.D. House, I.M. Robertson, M.D. Allendorf, Silver Cluster Formation, Dynamics, and Chemistry in Metal− Organic Frameworks, Nano letters 9 (2009) 3413-3418.
[15] M. Sabo, A. Henschel, H. Fröde, E. Klemm, S. Kaskel, Solution infiltration of palladium into MOF-5: synthesis, physisorption and catalytic properties, Journal of Materials Chemistry 17 (2007) 3827-3832.
[16] H.-L. Jiang, B. Liu, T. Akita, M. Haruta, H. Sakurai, Q. Xu, Au@ ZIF-8: CO oxidation over gold nanoparticles deposited to metal− organic framework, Journal of the American Chemical Society 131 (2009) 11302-11303.
[17] M. Müller, S. Hermes, K. Kähler, M.W. van den Berg, M. Muhler, R.A. Fischer, Loading of MOF-5 with Cu and ZnO nanoparticles by gas-phase infiltration with organometallic precursors: properties of Cu/ZnO@ MOF-5 as catalyst for methanol synthesis, Chemistry of Materials 20 (2008) 4576-4587.
[18] M.S. El-Shall, V. Abdelsayed, S.K. Abd El Rahman, H.M. Hassan, H.M. El-Kaderi, T.E. Reich, Metallic and bimetallic nanocatalysts incorporated into highly porous coordination polymer MIL-101, Journal of Materials Chemistry 19 (2009) 7625-7631.
[19] A. Dhakshinamoorthy, H. Garcia, Catalysis by metal nanoparticles embedded on metal–organic frameworks, Chemical Society Reviews 41 (2012) 5262-5284.
[20] H.R. Moon, D.-W. Lim, M.P. Suh, Fabrication of metal nanoparticles in metal–organic frameworks, Chemical Society Reviews 42 (2013) 1807-1824.
[21] A. Aijaz, A. Karkamkar, Y.J. Choi, N. Tsumori, E. Rönnebro, T. Autrey, H. Shioyama, Q. Xu, Immobilizing highly catalytically active Pt nanoparticles inside the pores of metal–organic framework: A double solvents approach, Journal of the American Chemical Society 134 (2012) 13926-13929.
[22] Q.-L. Zhu, J. Li, Q. Xu, Immobilizing metal nanoparticles to metal–organic frameworks with size and location control for optimizing catalytic performance, Journal of the American Chemical Society 135 (2013) 10210-10213.
[23] A. Carné-Sánchez, I. Imaz, M. Cano-Sarabia, D. Maspoch, A spray-drying strategy for synthesis of nanoscale metal–organic frameworks and their assembly into hollow superstructures, Nature chemistry 5 (2013) 203-211.

[24] L. Garzón-Tovar, M. Cano-Sarabia, A. Carné-Sánchez, C. Carbonell, I. Imaz, D. Maspoch, A spray-drying continuous-flow method for simultaneous synthesis and shaping of microspherical high nuclearity MOF beads, Reaction Chemistry & Engineering 1 (2016) 533-539.
[25] L. Garzón-Tovar, S. Rodríguez-Hermida, I. Imaz, D. Maspoch, Spray Drying for Making Covalent Chemistry: Postsynthetic Modification of Metal–Organic Frameworks, Journal of the American Chemical Society (2017).
[26] K.S. Park, Z. Ni, A.P. Côté, J.Y. Choi, R. Huang, F.J. Uribe-Romo, H.K. Chae, M. O'Keeffe, O.M. Yaghi, Exceptional chemical and thermal stability of zeolitic imidazolate frameworks, Proceedings of the National Academy of Sciences 103 (2006) 10186-10191.
[27] L. Lin, T. Zhang, H. Liu, J. Qiu, X. Zhang, In situ fabrication of a perfect Pd/ZnO@ ZIF-8 core–shell microsphere as an efficient catalyst by a ZnO support-induced ZIF-8 growth strategy, Nanoscale 7 (2015) 7615-7623.
[28] S. Ding, Q. Yan, H. Jiang, Z. Zhong, R. Chen, W. Xing, Fabrication of Pd@ ZIF-8 catalysts with different Pd spatial distributions and their catalytic properties, Chemical Engineering Journal 296 (2016) 146-153.
[29] S. Brunet, D. Mey, G. Pérot, C. Bouchy, F. Diehl, On the hydrodesulfurization of FCC gasoline: a review, Applied Catalysis A: General 278 (2005) 143-172.
[30] P. Baricelli, E. Lujano, M. Modrono, A. Marrero, Y. Garcıa, A. Fuentes, R. Sánchez-Delgado, Rhodium-catalyzed hydroformylation of C6 alkenes and alkene mixtures–a comparative study in homogeneous and aqueous-biphasic media using PPh 3, TPPTS and TPPMS ligands, Journal of organometallic chemistry 689 (2004) 3782-3792.
[31] M. Di Serio, M. Cozzolino, M. Giordano, R. Tesser, P. Patrono, E. Santacesaria, From homogeneous to heterogeneous catalysts in biodiesel production, Industrial & Engineering Chemistry Research 46 (2007) 6379-6384.
[32] M. Di Serio, R. Tesser, L. Pengmei, E. Santacesaria, Heterogeneous catalysts for biodiesel production, Energy & Fuels 22 (2007) 207-217.
[33] R. Yang, M. Su, M. Li, J. Zhang, X. Hao, H. Zhang, One-pot process combining transesterification and selective hydrogenation for biodiesel production from starting material of high degree of unsaturation, Bioresource technology 101 (2010) 5903-5909.
[34] S. Yang, J. Dong, Z. Yao, C. Shen, X. Shi, Y. Tian, S. Lin, X. Zhang, One-pot synthesis of graphene-supported monodisperse Pd nanoparticles as catalyst for formic acid electro-oxidation, Scientific reports 4 (2014).
[35] J. Cravillon, C.A. Schröder, H. Bux, A. Rothkirch, J. Caro, M. Wiebcke, Formate modulated solvothermal synthesis of ZIF-8 investigated using time-resolved in situ X-ray diffraction and scanning electron microscopy, CrystEngComm 14 (2012) 492-498.
[36] M. Shah, H.T. Kwon, V. Tran, S. Sachdeva, H.-K. Jeong, One step in situ synthesis of supported zeolitic imidazolate framework ZIF-8 membranes: Role of sodium formate, Microporous and Mesoporous Materials 165 (2013) 63-69.
[37] H. Kim, S. Das, M.G. Kim, D.N. Dybtsev, Y. Kim, K. Kim, Synthesis of phase-pure interpenetrated MOF-5 and its gas sorption properties, Inorganic chemistry 50 (2011) 3691-3696.
[38] S.-T. Wu, L.-S. Long, R.-B. Huang, L.-S. Zheng, pH-dependent assembly of supramolecular architectures from 0D to 2D networks, Crystal Growth & Design 7 (2007) 1746-1752.
[39] J. Cravillon, R. Nayuk, S. Springer, A. Feldhoff, K. Huber, M. Wiebcke, Controlling zeolitic imidazolate framework nano-and microcrystal formation: Insight into crystal growth by time-resolved in situ static light scattering, Chemistry of Materials 23 (2011) 2130-2141.
[40] I.B. Vasconcelos, T.G. da Silva, G.C. Militao, T.A. Soares, N.M. Rodrigues, M.O. Rodrigues, N.B. da Costa, R.O. Freire, S.A. Junior, Cytotoxicity and slow release of the anti-cancer drug doxorubicin from ZIF-8, RSC Advances 2 (2012) 9437-9442.
[41] Y. Hu, H. Kazemian, S. Rohani, Y. Huang, Y. Song, In situ high pressure study of ZIF-8 by FTIR spectroscopy, Chemical Communications 47 (2011) 12694-12696.
[42] W.P. Zhou, A. Lewera, R. Larsen, R.I. Masel, P.S. Bagus, A. Wieckowski, Size effects in electronic and catalytic properties of unsupported palladium nanoparticles in electrooxidation of formic acid, The Journal of Physical Chemistry B 110 (2006) 13393-13398.

[43] B. Richter, H. Kuhlenbeck, H.-J. Freund, P.S. Bagus, Cluster core-level binding-energy shifts: the role of lattice strain, Physical review letters 93 (2004) 026805.
[44] R.A. Hunsicker, K. Klier, T.S. Gaffney, J.G. Kirner, Framework zinc-substituted zeolites: Synthesis, and core-level and valence-band XPS, Chemistry of materials 14 (2002) 4807-4811.
[45] Y.E. Cheon, M.P. Suh, Enhanced Hydrogen Storage by Palladium Nanoparticles Fabricated in a Redox-Active Metal–Organic Framework, Angewandte Chemie 121 (2009) 2943-2947.
[46] S. Opelt, S. Türk, E. Dietzsch, A. Henschel, S. Kaskel, E. Klemm, Preparation of palladium supported on MOF-5 and its use as hydrogenation catalyst, Catalysis Communications 9 (2008) 1286-1290.
[47] D. Wang, Y. Li, One-pot protocol for Au-based hybrid magnetic nanostructures via a noble-metal-induced reduction process, Journal of the American Chemical Society 132 (2010) 6280-6281.
[48] B. Lim, H. Kobayashi, P.H. Camargo, L.F. Allard, J. Liu, Y. Xia, New insights into the growth mechanism and surface structure of palladium nanocrystals, Nano Research 3 (2010) 180-188.

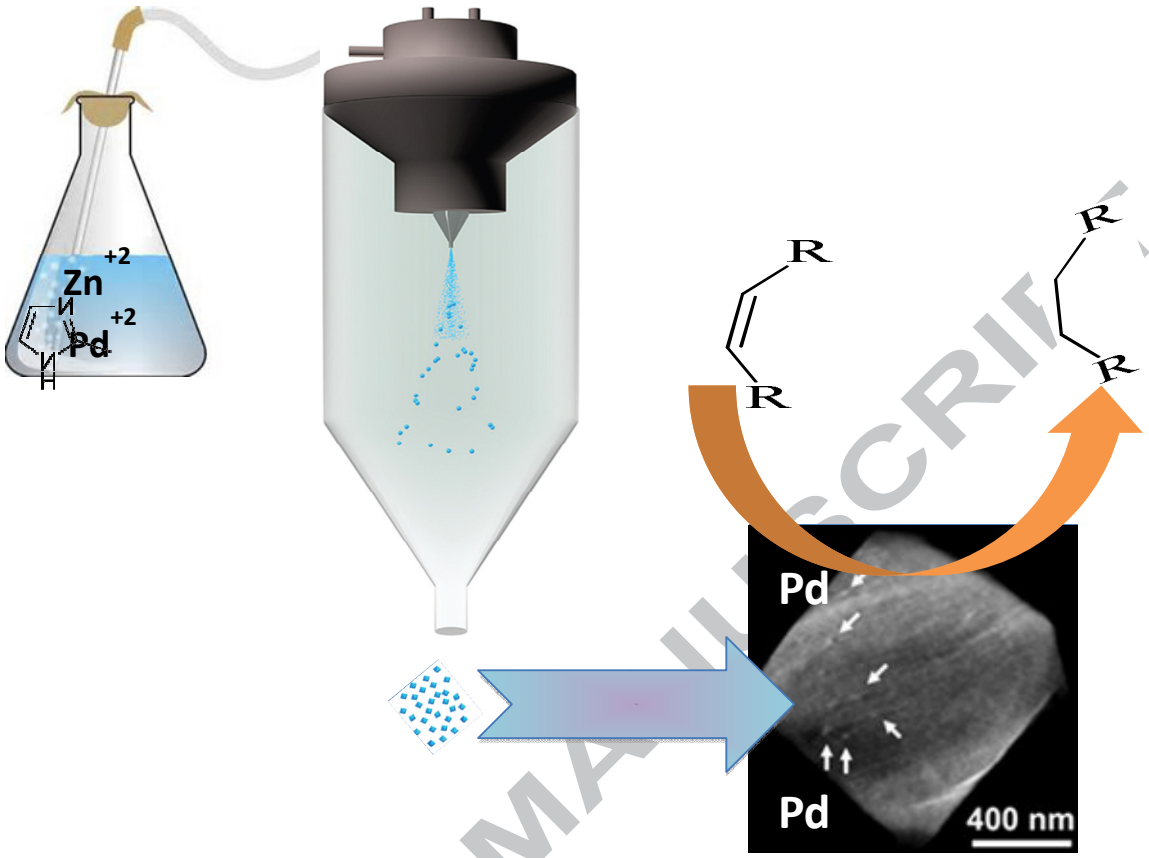

GA

Simultaneous Creation of Metal Nanoparticles in Metal Organic Frameworks via Spray Drying Technique

Nadia Gholampour[a], Somboon Chaemchuen[a], Zhi-Yi Hu[d], Bibimaryam Mousavi[a], Gustaaf Van Tendeloo[a,d], Francis Verpoort[a,b,c,*]

[a] State Key Laboratory of Advanced Technology for Materials Synthesis and Processing, Wuhan University of Technology, Wuhan, China

[b] *National Research Tomsk Polytechnic University, Lenin Avenue 30, 634050 Tomsk, Russian Federation*

[c] Ghent University Global Campus, Songdo 119 Songdomunhwa-Ro, Yeonsu-Gu, Incheon 406-840, South Korea.

[d] EMAT (Electron Microscopy for Materials Science), University of Antwerp, Groenenborgerlaan 171, 2020 Antwerp, Belgium

E-mail: Francis.verpoort@ugent.be

Highlights:

- Spray-dry technique was applied to synthesis Pd@ZIF-8.
- With this technique Pd@ZIF-8 was prepared without employing any stabilizer or surfactant.
- The synthesis procedure is included just one step.
- Characterization of pd@ZIF-8 demonstrated the presence of Pd nano-particles inside the ZIF-8 structure.
- Pd@ZIF-8 as a heterogeneous catalyst showed excellent activity in alkene hydrogenation.